



The Extent of Fault-Associated Modern Authigenic Barite Deposits Offshore Northern Baja California Revealed by High-Resolution Mapping

Roberto H. Gwiazda*, Charles K. Paull, David W. Caress, Christina Marie Preston, Shannon B. Johnson, Eve M. Lundsten and Krystle Anderson

Monterey Bay Aquarium Research Institute, Moss Landing, CA, United States

OPEN ACCESS

Edited by:

William W. Chadwick,
Pacific Marine Environmental
Laboratory (NOAA), United States

Reviewed by:

Samuel Yorks Johnson,
Pacific Coastal and Marine Science
Center, United States Geological
Survey, United States
John William Jamieson,
Memorial University of Newfoundland,
Canada

*Correspondence:

Roberto H. Gwiazda
rgwiazda@mbari.org

Specialty section:

This article was submitted to
Deep-Sea Environments and Ecology,
a section of the journal
Frontiers in Marine Science

Received: 26 March 2019

Accepted: 10 July 2019

Published: 02 August 2019

Citation:

Gwiazda RH, Paull CK,
Caress DW, Preston CM,
Johnson SB, Lundsten EM and
Anderson K (2019) The Extent
of Fault-Associated Modern
Authigenic Barite Deposits Offshore
Northern Baja California Revealed by
High-Resolution Mapping.
Front. Mar. Sci. 6:460.
doi: 10.3389/fmars.2019.00460

High-resolution mapping with an autonomous underwater vehicle (AUV) of a section of the San Clemente fault, offshore Southern California, reveals the largest documented cold-seep-associated barite deposits discovered to date. Although barite deposits along this fault, north of the mapped area, have been observed and sampled before in submersible dives, this study reveals massive newly found outcrops. The high-resolution surveys resolve their small-scale morphology, their large geographical extent and the structural controls on their emplacement. Detailed bathymetry (1 m × 1 m × 0.25 m grid resolution) of a ~12 km² area, ranging in water depths between 962 and 1,300 m and intersected by the fault, exhibits quasi-circular mounds of 10–30 m planar dimensions rising up to 11 m above the surrounding seafloor on a 30–45 m high and at least 1,100 m long ridge, and along truncated strata, but not along the main fault strand. Observations from a remotely operated vehicle (ROV) show that the mounds consist of steep sided dark-varnished blocks of barite. Active barite precipitation occurs as white friable spires emerging from the older deposits and as white porous precipitates filling fissures. Upward thinning spires and microbial mat occurrences atop the spires are consistent with aggradational growth due to precipitation from upward flowing solutions. Live *Lamellibrachia* tubeworms are found in association with the fissure-filling barite precipitates. Mapping surveys were also conducted along a short section of the San Clemente fault south of the Navy Fan. In addition, a 9 km² area along the San Diego Trough Fault south of the United States-Mexico border was mapped and visited in an ROV dive. In the three mapped regions sub-bottom chirp profiles indicate that often barite precipitation occurs where strata, truncated and uplifted by the fault, has thin or no sediment drape, allowing for Ba-rich solutions, that may have ascended through the main fault zone, to flow along bedding planes and mix with seawater sulfate at the seafloor interface. Despite the massive scale of the barite mounds,

they are not resolvable in surface ship multibeam-generated bathymetry (25 m grid resolution). As only a few areas have been mapped at the high-resolution employed in this study, the full extent of these deposits along the San Clemente Fault and other faults remains unknown.

Keywords: authigenic barite, barite deposits, high-resolution mapping, San Clemente fault, San Diego trough fault, cold seep barite, autonomous underwater vehicle, remotely operated vehicle observations

INTRODUCTION

Seafloor investigations of the California Borderland have occasionally revealed the presence of authigenic barite (BaSO_4) deposits. This evidence was collected by exploratory dredges and manned submersible dives (Revelle and Emery, 1951; Lonsdale, 1979; Torres et al., 2000, 2002; Hein et al., 2007). The most comprehensive studies were conducted on a barite outcrop on the San Clemente Fault, first visited by Lonsdale (1979) with the manned submersible *Seacliff*. Later, the same general area was investigated in dives with the manned submersible *Alvin* (Torres et al., 2002). Nevertheless, aside from visual descriptions, photographic images, and samples of barite deposits, the occurrence, geographical extent, structural relationship with faults, and detailed morphology of barite deposits on the California borderland are poorly known.

In addition to the cold-seep barite deposits along the San Clemente Fault, active cold-seep barite deposits in a range of sizes have been documented in several locations around the world. The largest occurrence is in the highly productive Derugin Basin in the Sea of Okhotsk where barite aggregates in column-shaped structures up to 10 m high occur scattered over an area of 22 km² in association with authigenic carbonate precipitates and chemosynthetic biological communities (Greiner et al., 2002; Aloisi et al., 2004). An association between exposure of old sediments to bottom waters and the occurrence of cold-seep barite deposits has been noted in several locations. In the Peru Margin, barite deposits were found at sites of fluid seepage along two several-hundred meters tall escarpments and a canyon wall where slope failures exposed older sediment sequences to bottom water (Torres et al., 1996a; Aquilina et al., 1997). Similarly, cold-seep barite precipitates were found in Tubeworm Slump (Naehr et al., 2000), a slide scar on the floor of the highly productive Monterey Bay, offshore California, where old sediment sequences are exposed to bottom seawater. Other known locations with cold-seep barite deposits of a more diffuse character and/or with smaller buildups are the Gulf of Mexico (Feng and Roberts, 2011), Alaska (Suess et al., 1998) and Gulf of California (Canet et al., 2013). Torres et al. (2003), summarized the sequential processes leading to the formation of cold-seep barite deposits: enhanced barium and carbon flux associated with high productivity on overlying waters; remobilization of barium in reduced pore waters devoid of sulfate due to consumption by methane, and precipitation of barite when reduced fluids rich in Ba are exposed to oxic, sulfate-rich bottom waters.

The accumulation of barite at fault-associated cold-seeps is believed to be a modern analog to Paleozoic and older stratiform barite ore deposits, which are the most important

source of industrial barite (Clark et al., 2004). This association is based on their similarity in barite crystallography, barite crystal arrangement texture, lack of polymetallic sulfides, lithological character of hosting strata, and association with faults or steep slopes (Torres et al., 2003). Tectonically active basins near continental margins are considered to be suitable environments for the accumulation of these deposits (Torres et al., 2003; Koski and Hein, 2004). In such settings, tectonic motions displace, uplift and expose older organic-rich reduced sediments to bottom seawater. Active flow of Ba-rich fluids to the seafloor creates favorable conditions for the precipitation of authigenic minerals because ascending waters mix with bottom seawater having a different redox and chemical saturation state.

Here we report new discoveries in the California Borderland of barite deposits of a large geographical and vertical extent. During the course of high-resolution mapping with an autonomous underwater vehicle (AUV) to document recent movements along the dextral strike-slip faults that form the transform boundary between the Pacific and North American plates offshore southern California, barite deposits were discovered along segments of the San Clemente Fault and of the San Diego Trough Fault zones (**Figure 1A**). The mapped sections had been selected for higher resolution mapping based on previously collected surface-ship multibeam data that suggested the presence of scarp lineaments indicative of recently faulted strata. In the newly surveyed segment of the San Clemente Fault the high-resolution map reveals kilometer-scale patches of a very rugged morphology. Subsequent inspection with a remotely operated vehicle (ROV) confirmed that the rough bathymetry was composed of massive columnar deposits of authigenic barite. Furthermore, one of these surveys partially covered the site where the earlier observations of barite outcrops had been made. In addition, barite was also found on the San Diego Trough Fault zone. Here we document the morphology and extent of these deposits, as well as their occurrence in relation to the imaged fault segments.

MATERIALS AND METHODS

High-resolution maps and sub-bottom chirp profiles were collected during three AUV surveys, followed by ROV dives at two of the AUV mapped sites (**Figure 1A**). The AUV designed by the Monterey Bay Aquarium Research Institute (MBARI) carried a 200 kHz multibeam sonar and a 1–6 kHz chirp sub-bottom profiler. The vehicle navigated 50 m above the seafloor at a speed of 3 knots for 18 h along predefined lines spaced ~150 m apart. The overlap between swaths was 60 m. Multibeam data were processed with the software package MB-System (Caress et al.,

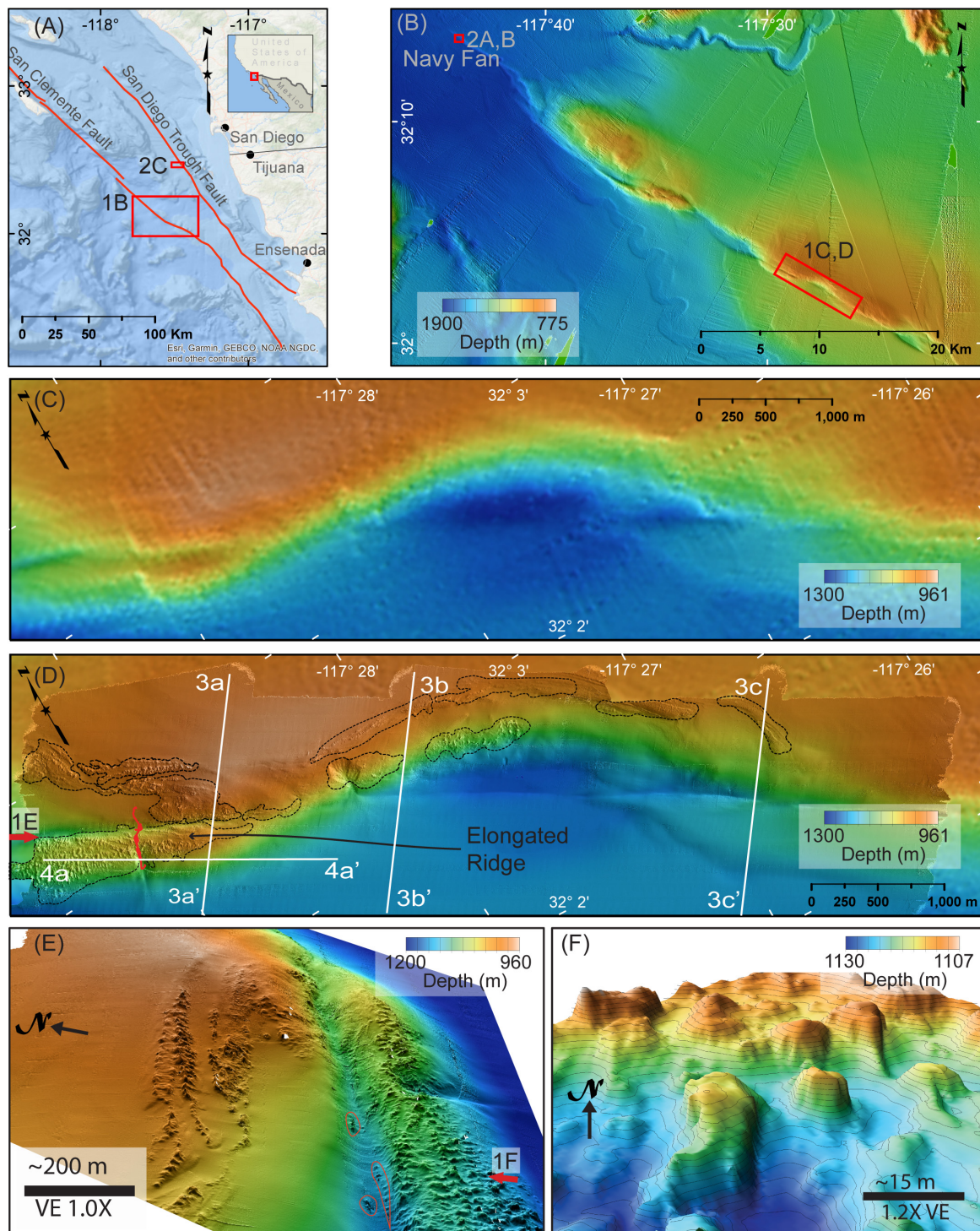


FIGURE 1 | (A) Regional map showing study area offshore California and Mexico's border. **(B)** Surveyed sections of the San Clemente Fault. Red squares identify the locations of **C,D**, **Figures 2A,B**. **(C)** Bathymetry from surface-ship multibeam data of the main area surveyed along the San Clemente Fault. Resolution is 25×25 m. **(D)** Bathymetry from AUV data of the same area shown in **C**. Resolution is $1 \times 1 \times 0.25$ m. The red line is the path of ROV dive DR767. White lines are the traces of chirp sub-bottom profiles shown in **Figures 3, 4**. Black dashed lines encircle areas with rough morphology indicative of barite mounds. Red arrow shows the direction of the perspective view shown in **E**. **(E)** A perspective view showing the rough morphology and central depression where the main strand of the San Clemente fault is presumably located. Abundant barite mounds are found on the elongated ridge south of the main strand of the fault and along strata on the top of the escarpment north of it. Red lines encircle linear arrangements of barite deposits found on the central trough that are parallel to the main strand of the fault. **(F)** A perspective view of barite mounds south of the trough, zoomed in, and vertically exaggerated to show individual mounds. Contours are 2 m.

2008) to generate grids with a resolution of $1\text{ m} \times 1\text{ m} \times 0.25\text{ m}$. The chirp profiles have a vertical resolution of 10 cm and can image up to $\sim 40\text{ m}$ sub-bottom depths. Video observations and samples were subsequently collected using MBARI's ROV *Doc Ricketts*.

AUV survey-1 was conducted along the San Clemente Fault on a $6\text{ km long} \times 1.9\text{ km wide}$ section of the seafloor centered at $32.0433^\circ\text{N } 117.4632^\circ\text{W}$ over a water depth range of 962 to 1,300 m (**Figure 1D**). ROV dive DR767 was also conducted on this segment of the fault guided by the AUV map (**Figure 1D**). AUV survey-2 was conducted further north along the San Clemente Fault in the Navy Fan (**Figure 1B**). In **Figures 2A,B** we present a map and perspective view of a small 0.25 km^2 area in the Navy Fan that is just slightly north of the site along the San Clemente Fault where the presence of barite deposits in the California Borderland was first described (Lonsdale, 1979; Torres et al., 2000, 2002). The full extent of the Navy Fan AUV map is in Carvajal et al. (2017). AUV survey-3 took place over a $5.7 \times 1.6\text{ km}$ section of the San Diego Trough Fault just south of the United States-Mexico border (**Figures 1A, 2C**). A subsequent ROV dive (DR769) encountered outcrops of barite on the flanks of a ridge abutting the fault trough (**Figure 2C**). No temperature probe was deployed from the ROV in either dive.

Eight rock samples were collected in the ROV dives [San Clemente Fault ($n = 6$) and San Diego Trough Fault ($n = 2$)]. Strontium isotopes of the rock samples were measured by Actlabs, Ontario, Canada, via multicollector ICP-MS after hot sodium peroxide fusion, following the procedure described in Holmden et al. (1997). Long term external precision was ± 0.00002 (2σ) for the $^{87}\text{S}/^{86}\text{Sr}$ ratio based on repeated analyses of SRM 987. Sulfur isotopes of barite and carbon isotopes of carbonate were measured by Isotech laboratories Inc., Illinois, United States. Isotope ratios are expressed in delta notation (per mil deviation from the isotopic ratio of a standard) using the Vienna Canyon Diablo Troilite standard (VCDT) and the Vienna Pee-Dee Belemnite (VPDB) as standards for sulfur and carbon isotope ratios, respectively. Long term reproducibility of isotopic measurements at Isotech laboratories, Inc., is 0.5% (1σ) for $\delta^{34}\text{S}$, and 0.3% (1σ) for $\delta^{13}\text{C}$. Mineral composition was analyzed by powder X-ray diffraction by Metallurgical Engineering Services Inc., Richardson, Texas. Concentrations of trace elements, chalcophile elements and REE were measured by Actlabs, Ontario, Canada, by ICP-MS after lithium metaborate/tetraborate or hot sodium peroxide fusion, and by neutron activation analyses. Measurements of standard reference materials yielded concentrations inaccuracies of less than 25% in 90% of the of the elements measured (**Supplementary Table S1**).

Microbial mats were peeled off rocks collected by the ROV using tweezers, then stored at -80°C until processed. Genomic DNA from several replicates was isolated with a PowerSoil®DNA isolation Kit (MO BIO Laboratories, Carlsbad, CA, United States). Genomic DNA was used for Illumina MiSeq high-throughput amplicon sequencing (Illumina Inc., San Diego, CA, United States) using the 16S rRNA V4 primers 515F (Parada et al., 2016) and 806R (Caporaso et al., 2010, 2011) with Illumina adapters and barcodes per methods of the Earth Microbiome

Project (Thompson et al., 2017). Data were analyzed using QIIME 2 (Caporaso et al., 2011).

RESULTS

AUV Mapping

AUV survey-1 mapped a 6 km long area traversed longitudinally by the strike-slip San Clemente Fault. The AUV map and the map obtained from surface ship multibeam data¹ (**Figures 1C,D**) both show the major topographic features in this area: The area is bisected by a linear trough, with the northern side dominated by a 245 m high escarpment (slope $\sim 22^\circ$) and the southern side displaying a central basin and a narrow elongated ridge to the west. However, the AUV-generated map is rich in details not discernible in the surface ship multibeam grid, most notably the large patches of distinctly rough surface morphology.

The high-resolution map shows the rough surface is composed of a field of closely clustered large mounds on the elongated ridge at the western corner of the mapped area (lower left quadrant **Figures 1D,E**). The mound morphology consists of quasi-circular to elongated features, with planar dimensions ranging from 10 to 30 m and heights up to 11 m above the surrounding seafloor (**Figure 1F**). Mounds cover up to 50% of the seafloor area of the $300\text{ to }550\text{ m wide}$ ridge which rises 30 to 45 m above the surrounding seafloor. Some mounds appear to preferentially occur in rows which run parallel to the trough where the main strand of the San Clemente Fault is presumably located (**Figure 1E**). The linear arrangement of the mounds is more evident on the northern side of the fault where they appear to follow the truncated strata exposed along the upper section of the escarpment (**Figures 1E, 3**). Mounds also occur in several other patches along the face of the escarpment that slopes from the north toward the inferred main fault trace (**Figure 3**). However, this morphology is not present along the main fault trace.

A row of 2–3 m tall cones along the foot of a scarp on the Navy Fan, as well as scattered $\sim 1\text{ m high}$ lumps on the scarp face, were imaged at the edge of AUV survey-2 (**Figure 2A**). These features are just 500 m further northwest along the trace of the fault from the $\leq 4\text{ m high}$ mounds found by Lonsdale (1979) and 3 km from the 1 m high mounds observed on *Alvin* dives (Torres et al., 2000, 2002). The size of individual mounds and their geographical extent in this segment of the San Clemente Fault are apparently considerably reduced compared to their size and distribution at the new site discovered in the San Clemente Fault in AUV survey-1, 31 km further to the southwest (**Figure 1D**).

A section of the San Diego Trough Fault just south of the United States-Mexico border was mapped in AUV survey-3 (**Figures 1A, 2C**). The fault zone manifests on the seafloor as a distinct linear depression bisecting the survey area in a north-northwest to south-southeast direction. The bathymetry is dominated by a set of push-up ridges and pull apart basins created by motion along the fault. Rough seafloor textures like those imaged along the San Clemente Fault were not detected

¹<https://www.ngdc.noaa.gov/mgg/bathymetry/relief.html>

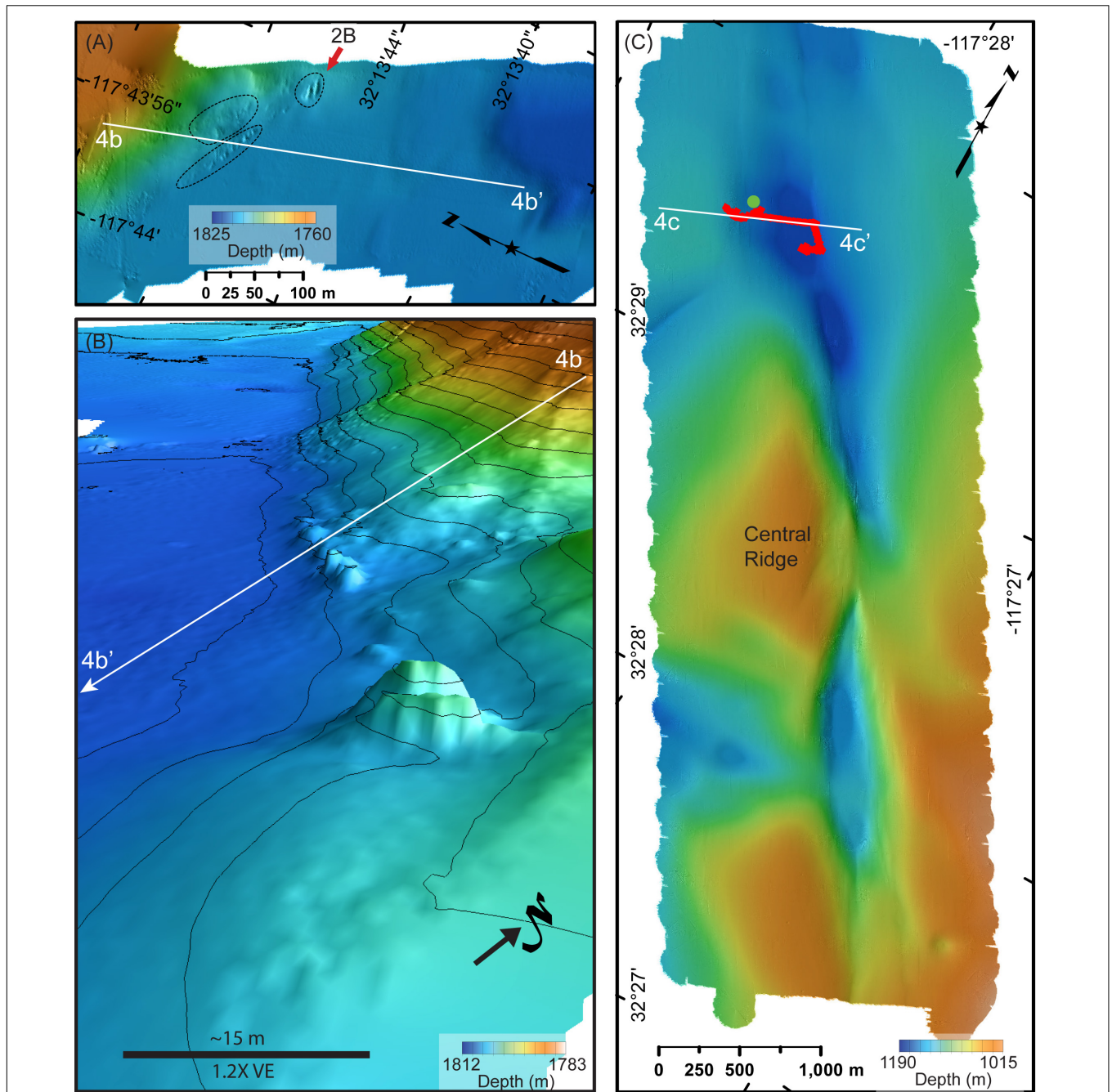


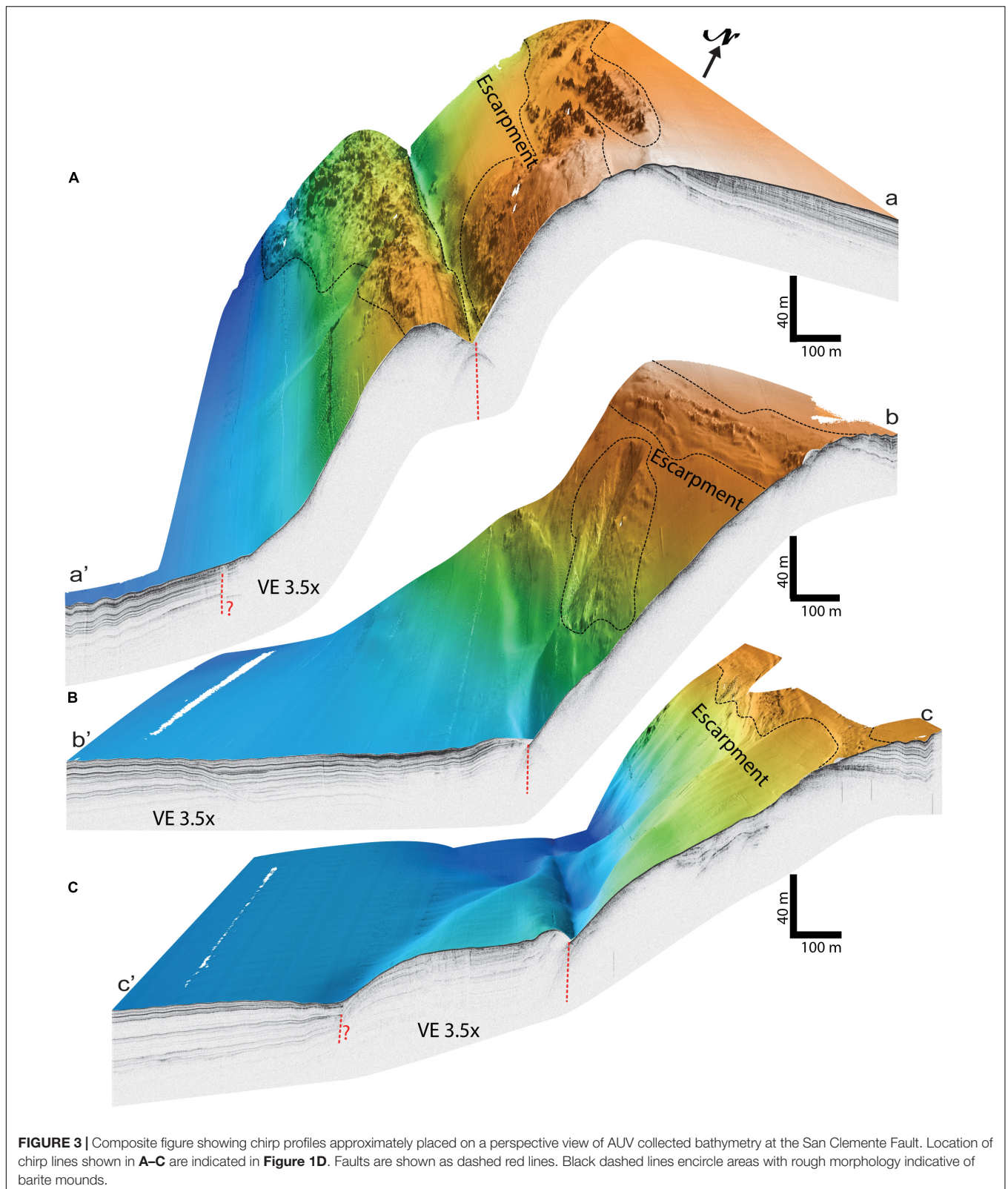
FIGURE 2 | (A) A small section of AUV collected bathymetry on the San Clemente Fault in the Navy Fan area. Black dashed lines encircle areas with rough morphology indicative of barite mounds. Red arrow indicates the direction of the perspective view shown in panel **B**. White line is the location of the chirp sub-bottom profile shown in **Figure 4B**. **(B)** A perspective view of the mounds on the escarpment above the San Clemente Fault. Contours are 2 m. White line is the location of the chirp sub-bottom profile shown in **Figure 4B**. **(C)** AUV collected bathymetry on a section of the San Diego Trough Fault. The red line shows the path of ROV dive DR769. The green dot indicates the location of a barite deposit. White line is the location of the chirp sub-bottom profile shown in **Figure 4C**.

in this survey including the location where barite outcrops were observed in ROV dive DR769 (see below) (**Figure 4C**).

Chirp Profiles

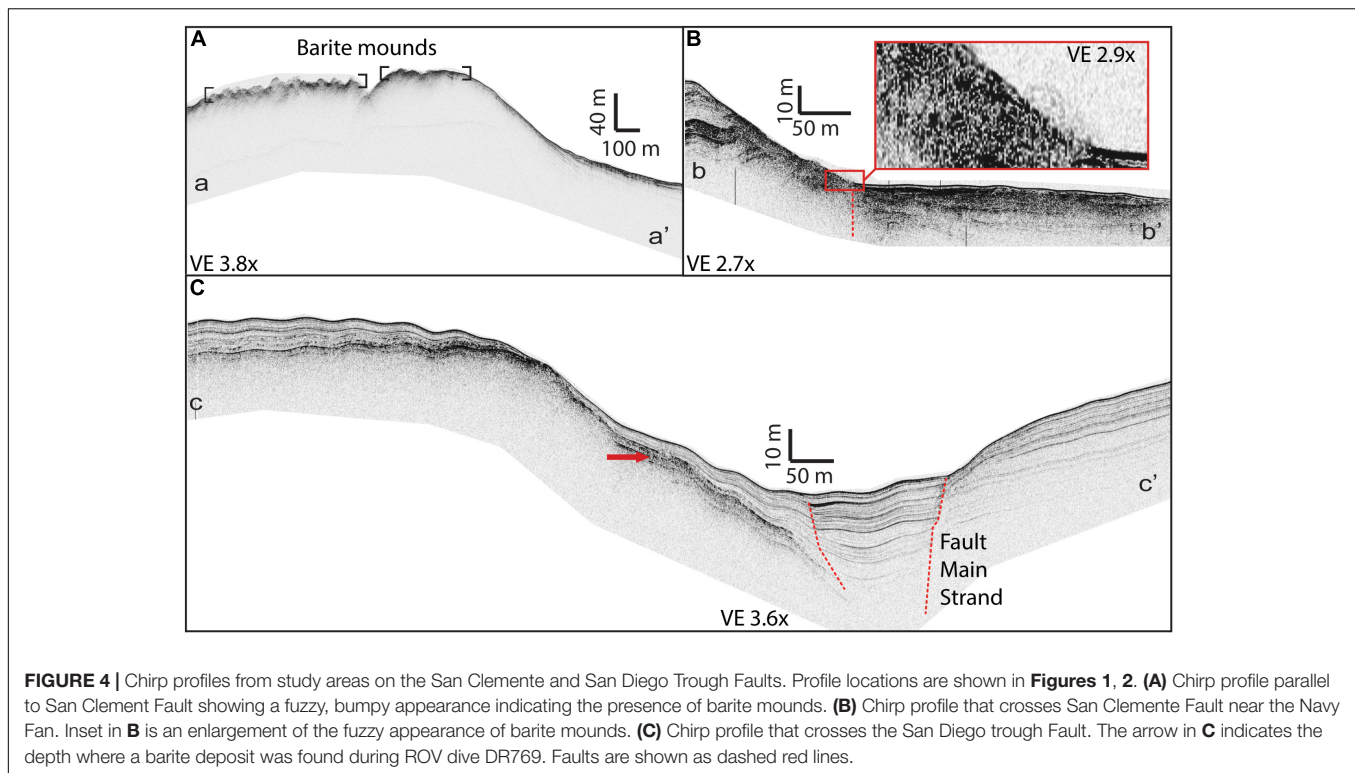
A profile across the San Clemente Fault zone in AUV survey-1 shows that the large mound structures on the elongated ridge

appear as a diffuse bumpy fuzz above the seafloor reflection (**Figure 4A**, profile trace 4a–4a' in **Figure 1D**). Strata uplifted by motion along the fault is documented in the chirp profiles. A profile normal to the fault shows that the dips of the strata on both sides of the fault trough are different and oriented away from the trough (**Figure 3A**, profile trace 3a–3a' in **Figure 1D**). On the



northern side of the fault trough, layered sediments are visualized on top of the ridge with an apparent 4° dip to the northeast. Profiles from the nearly flat basin floor on the southern side of the

fault zone show up to 40 m of layered sediments which dip 4.5° to the southwest as they approach the main strand of the fault, and either pinch out or lap up on the flank of the ridge before



losing lateral continuity (**Figure 3A**). Interruption of these strata by a fault as they approach the ridge is also possible, however, no significant vertical offset of the layered sediment is observed.

Unequivocally establishing whether the San Clemente Fault is single or multiple stranded where the rough morphology is present is not possible. The narrow depression running along the center of the survey (**Figure 1D**) and delineated by upturned sediment layers in chirp profiles (**Figure 3C**) is obviously the main strand of the fault. However, there is no clear evidence, such as displaced reflectors or offset of piercing points, for the presence of other major fault strands. The appearance of rough topography along the top of the escarpment north of the main fault strand is coincident with truncated strata in all chirp profiles (**Figure 3**).

A chirp line across the San Clemente Fault on the Navy Fan (profile trace 4b–4b' shown in **Figures 2A,B**) shows that the locations of the mounds on the high-resolution map correspond to the section of the escarpment (slope $\sim 11^\circ$) where the sediment drape thickness is minimal (**Figure 4B**). The mounds at the scarp base, which are clearly imaged in the AUV bathymetry (**Figure 2A**), again only appear as a diffuse fuzz above the seafloor reflector (**Figure 4B**, inset).

Sub-bottom profiles from the San Diego Trough Fault (profile trace 4c–4c' in **Figure 2C**) show thick layered sediment accumulating in all areas except over the steepest slopes (**Figure 4C**) and the top of the central ridge (not shown). The chirp line over which ROV dive DR769 was conducted shows a thick accumulation of layered sediment in the ponded basin, which is disrupted by the main trace of the fault. On the western

side of the fault, a barite outcrop was found (see below) where sediment drape thins out upslope on the escarpment.

ROV Dives

Doc Ricketts dive DR767 was conducted on the San Clemente Fault at the southwest corner of the mapped area (left lower quadrant, **Figure 1D**), along a transect that ascended the elongated ridge with the mound morphology, descended to the main fault strand and continued up some of the escarpment on the northern side of the fault (**Figure 1D**). Visual inspection showed that the flanks and tops of the mounds on both sides and top of the southern elongated ridge are composed of aggregates of meter-scale rough-textured clumps (**Figures 5A–C**), hereafter called “heads.” The mounds appear to have formed by consolidation of multiple heads along with shed debris. Individual heads are typically dark-varnished, but occasionally are bright white and emerge from either the top or along the sides of the mounds. Chemical analyses of collected samples indicate that the white aggregates are composed of barite. They typically occur as a single mass at the bottom that both widens and branches upward (**Figures 5B,C**). The branches further narrow into upward pointing fingers, which are in places topped by microbial mats (**Figure 5D**). In places, gelatinous microbial mats completely cover the top of the heads with filaments extending into and seen fluttering in the surrounding water (**Figure 5E**). White barite aggregates are also found filling fissures or fractures between the larger dark-varnished blocks of apparently older heads. No shimmering waters were observed that would visually indicate outflow of fluids warmer than bottom waters.

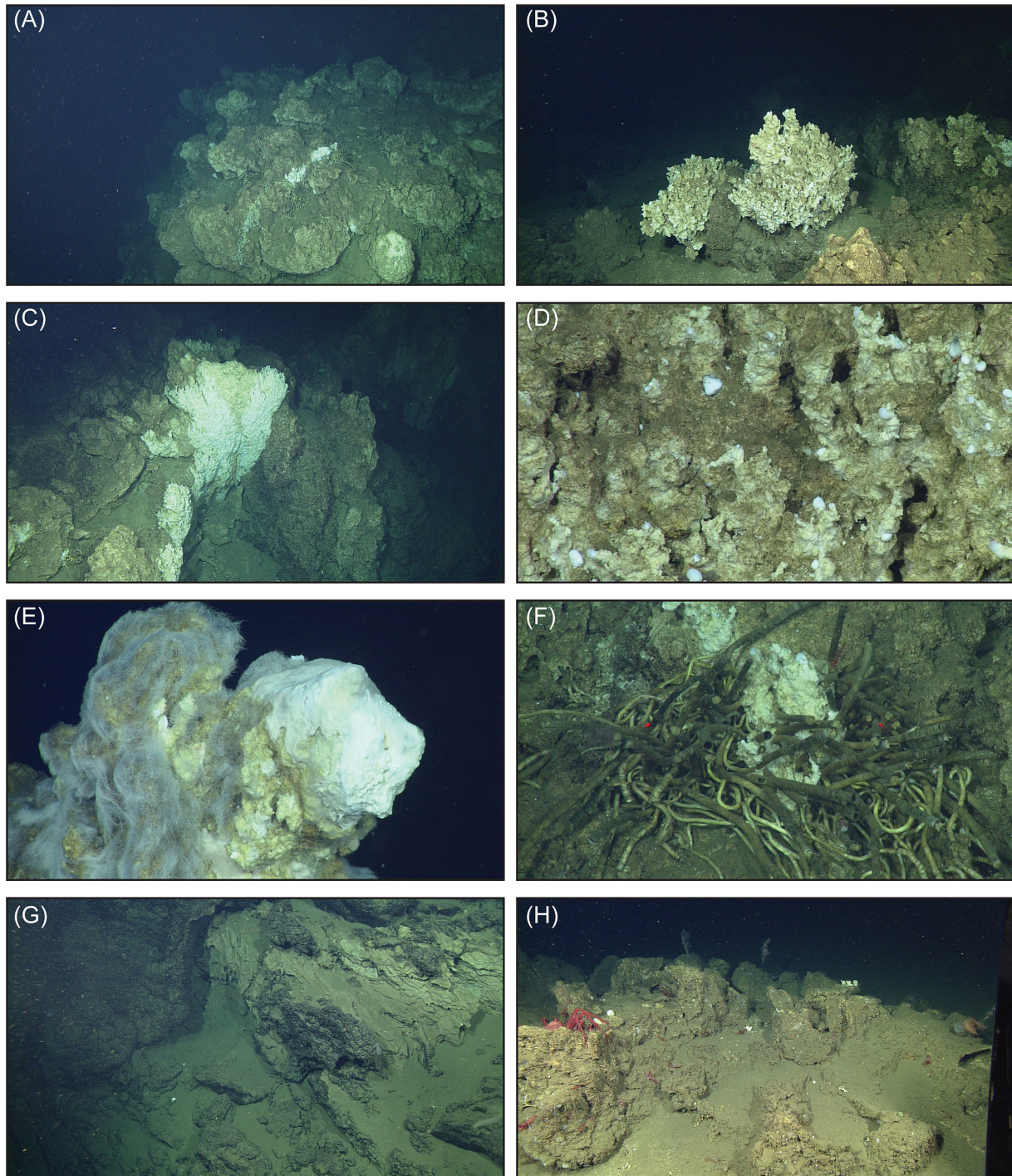


FIGURE 5 | Images collected during ROV dives DR767 and DR769 on the San Clemente Fault and San Diego Trough Fault, respectively. **(A,B)** Barite mounds of presumably different ages as indicated by the accumulation of a muddy drape. **(C)** Barite “heads” with spires ending in “fingers,” growing from the sides and top of a barite mound. **(D)** Bacterial mats growing at the ends of barite “fingers.” **(E)** Filamentous and gelatinous bacterial mats fully covering a barite “head.” **(F)** Barite precipitates engulfing live *Lamellibrachia* tubeworms. Red dots are laser beams separated by 29 cm. **(G)** Sub-horizontal layers of cemented drape intercalated with barite deposits. To the left a barite deposit is draped over the cemented strata. **(H)** Barite deposit found near the San Diego Trough Fault.

Scattered clusters of *Lamellibrachia* tubeworms are present in association with the white precipitates, and in cracks between the darker barite deposits (**Figure 5F**). In some instances,

these apparently living tubeworms are engulfed by the mineral precipitates. Sessile megafauna typical of hard-substrate surfaces, such as corals and sponges, is noticeably absent.

In the depressions between mounds there is some rubble derived from the mounds along with shell hash and some hemipelagic sediment drape (Figure 5G). However, sediment drape is almost absent on the elevated parts of the mounds. No significant pavements of authigenic carbonate characteristic of methane seeps were observed. Outcrops of sub-horizontal beds of light-colored barite-cemented sediment drape (sample DR767 Rx-4, Table 1) are also exposed on both sides of the elongated ridge (Figure 5G). Barite heads were found in places draped over exposed outcrops of sub-horizontal bedding (Figure 5G).

The mapped area of the San Diego Trough Fault was explored during ROV dive DR769. Two small < 1 m high outcrops were found at a depth of 1172–1175 m (Figure 5H), where the sediment drape thins out on the western flank of the trough (Figure 4C). Chemical analyses confirmed these heads were composed of friable barite with a yellowish interior, similar to those collected along the San Clemente Fault in dive DR767. Earlier in the dive the ROV navigated along the trace of the fault before climbing the ridge to the west (Figure 2C), but did not find other barite deposits along the fault or along the sediment drape covered lower part of the slope.

No ROV dives were conducted on the mounds mapped in the Navy Fan (Figures 2A,B).

Geochemistry

Five of the six rock samples collected in the San Clemente Fault ROV dive came from the heads and are composed of very porous and friable aggregates of euhedral to sub-euhedral sub-millimeter weakly cemented crystals. The sixth is a sample of the light-colored sub-horizontal cemented drape found intercalated with the massive blocky deposits on the SW facing slope of the ridge (Figure 5G). Based on mineral and elemental analyses, the precipitated white heads are composed of at least 80% by weight barite, with the remainder composed of varying amounts of clays, pyrite and aragonite.

The average $^{87}\text{Sr}/^{86}\text{Sr}$ ratio of Sr in barites collected in the San Clemente Fault dive is 0.708576 (range 0.70822–0.70898) (Table 1). The average $\delta^{34}\text{S}$ of the barite samples from the same dive is 23.8‰ relative to VCDT (range 22.4–24.8‰), but the $\delta^{34}\text{S}$ of barite in the light-colored sub-horizontal cemented drape is 43.5‰. This sample (DR767 Rx-4) is made of non-porous calcium carbonate with barite filling spaces and veins adding up to 10% content by weight. The $\delta^{13}\text{C}$ of the carbonate is –24.7‰ relative to VPDB.

The two San Diego Trough Fault samples had $^{87}\text{Sr}/^{86}\text{Sr}$ ratios of 0.70848 and 0.70860, within the range of $^{87}\text{Sr}/^{86}\text{Sr}$ ratios measured in the San Clemente Fault barites, and their $\delta^{34}\text{S}$ values of 27.5 and 24.6‰ are close to the $\delta^{34}\text{S}$ of the barite rich samples from the San Clemente Fault.

The concentrations of chalcophile elements are low (Supplementary Table S1). The trace element and rare element concentrations are within the concentration ranges of barite samples dredged from the seafloor offshore Southern California and barites recovered on the San Clemente Fault by Alvin, as reported by Hein et al. (2007). No significant differences were found between the chemical composition of samples from the San Clemente Fault and from the San Diego Trough Fault zones.

16S ribosomal RNA gene sequencing of the filamentous and gelatinous mats indicated the presence of both sulfur- and methane- cycling microorganisms, many commonly found in microbial mats and seafloor sediments (Dhillon et al., 2003; Schauer et al., 2011; Salman-Carvalho et al., 2016). Fifty percent of the sequences were similar to epsilonproteobacteria (Helicobacteraceae), gammaproteobacteria (Beggiatoa), and deltaproteobacteria (Desulfobacteraceae). Much rarer (<1%) were sequences affiliated with methane-cycling including Methylococcales, AMNE-1, AMNE-2c, and Methanobacteria.

DISCUSSION

The highly detailed mapping of the distinctive rough topography in AUV surveys on the San Clemente Fault reveals the most extensive authigenic barite deposits discovered to date (Figure 1D). These deposits at 962 to 1,300 m water depth are not discernible with currently available surface-ship multibeam mapping technology (Figure 1C). However, the enhanced resolution of AUV surveys (Figure 1D) allowed for the serendipitous discovery of the large extent, both in geographic and vertical scales, of barite deposits along just one 6 km section of the San Clemente Fault. Furthermore, by chance a small cluster of barite heads were found during an ROV dive in the San Diego Trough Fault in a setting structurally similar to that of the San Clemente Fault. These occurrences further the interpretation that authigenic barite deposits are associated with active fault zones and suggest barite deposits may also occur along other faults of the California Borderland where certain required structural criteria are met.

Structural Controls on Barite Accumulation

The structural elements that control the emplacement of these barite deposits are illustrated in the high-resolution maps, sub-bottom profiles, and ROV observations. The morphology of the spires and the location of bacterial mats are consistent with an upward flow of solutions that promote aggradational growth of barite at the top of the spires, suggesting the outflow of a buoyant fluid.

The massive bodies of barite appear to have formed on the seafloor as a composite of individual heads that are cemented into mounds by new barite precipitate filling gaps between adjacent heads. While no chemical analyses were conducted on the dark surface coating of the mounds, Lonsdale (1979), describes the dark varnish of the barite mounds found in the Navy Fan as a 1 mm-thick Mn-oxide precipitate, and proposed that it occurred after the outflow of barite precipitating fluid has ceased. Thus, the varnish coating on the mounds would attest to their longer exposure to seawater.

The AUV surveys show that barite deposits are typically associated with escarpments having thin or non-existent sediment drape. In the San Clemente Fault section outcropping near the Navy Fan (Figure 2B), steep-sided mounds emerge at the foot of the escarpment, and smoother mounds are visible farther up on the slope along the northern side of the fault

TABLE 1 | Isotopic values.

Sample	Location	$^{87}\text{Sr}/^{86}\text{Sr}$ barite \pm 2SE	$\delta^{34}\text{S}$ barite, %	$\delta^{13}\text{C}$ carbonate, %
DR767 Rx-1	San Clemente Fault	0.70898 \pm 0.00002	24.3	
DR767 Rx-2	San Clemente Fault	0.70860 \pm 0.00002	24.8	
DR767 Rx-3	San Clemente Fault	0.70822 \pm 0.00002	22.4	
DR767 Rx-4	San Clemente Fault	0.70894 \pm 0.00002	43.5	-24.7
DR769 Rx-1	San Diego Trough Fault	0.70848 \pm 0.00002	27.5	
DR769 Rx-2	San Diego Trough Fault	0.70860 \pm 0.00003	24.6	

where sediment cover diminishes, but are absent on the southern side of the fault where sediment cover is thicker. In the main San Clemente Fault survey area, the barite mound morphology along the top of the escarpment on the north side of the fault (Figure 1E) clearly follows the horizons of truncated strata where no sediment drape is seen in chirp profiles (Figure 3). In the San Diego Trough Fault, the thickest recent sediment accumulations are along the trace of the fault and no barite mounds were detected there, whereas the barite deposit found at this site is on the escarpment with comparatively thin sediment cover (Figure 4C). The barite deposits occur where upturned and truncated strata are exposed or have minimal sediment cover.

The arrangement of barite deposits on or along truncated strata suggests the primary conduits for buoyant Ba-rich solutions to reach the seafloor are dipping bedding planes. Lateral variations in heat flow can be sufficient to stimulate weak fluid circulation through sedimentary cover (Langseth et al., 1988). Ba-rich reduced fluids migrating along relatively permeable bedding planes conduits form cold-seep barite deposits when they encounter oxic sulfate-rich bottom waters. A similar mechanism was proposed for barites found in Monterey Bay (Naehr et al., 2000) and the Peru Margin (Torres et al., 1996a), but instead of faulting, in those studies slope failures caused the truncation of bedding planes and their exposure to bottom waters. In the California Borderland, exposure of truncated beds from tectonic displacements along faults is facilitating the formation of barite deposits.

Interestingly, no fluid flow to the seafloor appears to take place along the main strand of the fault in the mapped sections of the San Clemente and the San Diego Trough Faults (Figure 4C) because no barite deposits were found along their morphologically obvious main traces. However, while there do not appear to be surface accumulations of barite along the main faults, faults may facilitate the ascent of solutions from depth that later diffuse and reach the seafloor along bedding planes.

Precipitation of barite from Ba-rich solutions when they reach the seafloor is consistent with the aggrading structures documented in the ROV dives and the geochemical signals of samples collected here and elsewhere along the San Clemente Fault (Torres et al., 2003). The $\delta^{34}\text{S}$ of the massive barite deposits (range 22.4–24.8%) is close to the seawater value of 21.1%, which indicates that barite precipitated close to the seafloor, and not in oxygen depleted pore waters within the sediment column where $\delta^{34}\text{S}$ of sulfate would have been significantly enriched due to the loss of isotopically light sulfur via reduction. Nevertheless, some barite cementation appears to take place

in the subsurface. The sample of barite with a $\delta^{34}\text{S}$ value much more positive than seawater (DR767 Rx, $\delta^{34}\text{S}$ = 43.5%) occurs in association with carbonate partially derived from biogenic methane (carbonate $\delta^{13}\text{C}$ = -24.7%) (Paull et al., 1992). The mineral association between barite and methane-derived carbonate and the heavy sulfur isotopic composition are consistent with barite precipitation deeper within the sediment after substantial sulfate reduction.

Cold-Seep Environments With High Rates of Barite-Mineralization

Aloisi et al. (2004), attributed the formation of barite chimneys and the uncharacteristic absence of authigenic carbonate to comparatively high seepage rates of Ba-rich solutions. Rapid formation of the barite mounds can also account for the lack of sediment drape, as newly formed barite deposits incorporate or cover recently accumulated sediment material. Precipitation of barite in the subsurface normally occurs at the depth of the sulfate-methane boundary where ascending solutions rich in barium and methane encounter sulfate-rich porewaters (Torres et al., 1996b; Snyder et al., 2007) leading to barite and authigenic carbonate precipitation. The absence of carbonate precipitation might be due to seepage rates high enough to move the sulfate-methane boundary toward the sediment-water interface where methane could escape, minimizing its rate of conversion to bicarbonate, and ultimately to carbonate precipitation (Aloisi et al., 2004). Barite formation would take place closer to the seafloor and at a rate that surpasses the sedimentation rate, leading to the formation of barite columns raising above the seafloor and thus preventing the accumulation of layered hemipelagic drape.

The absence of fauna typically found on hard bottom substrates (e.g., corals and sponges) as well as chemosynthetic clams is notable. The absence of clams could be due to lack of soft substrates for anchoring. Of all known chemosynthetic vesicomyid clams, only "*Calyptogena magnifica*" is known to inhabit hard substrates (Johnson et al., 2017). The absence of corals and sponges raises the possibility that the barite mound environment is deleterious to these fauna. The existence of fine particle barite suspensions has been hypothesized for the San Clemente basin (Torres et al., 2002), and fine barite particle exposure has been shown, at least in some sponges, to produce adverse effect (Fang et al., 2018).

The rate of growth of surface barite appears to be comparatively rapid. *Lamellibrachia* tubeworms were found

engulfed by fissure-filling barite (**Figure 5G**) indicating that the local rate of growth of authigenic barite on the surface deposits is of the same order as the rate of growth of the tubeworms. *Lamellibrachia* tube worms living in hydrocarbon seeps have been found to grow at variable rates, on the order of a few centimeters per year (Bergquist et al., 2000). Assuming similar order of magnitude rates for the tubeworms found here, the fact that barite precipitates were found in one instance surrounding the upper 3 cm of some living tubeworms indicates that cm/year is a plausible rate of growth of barite surrounding active seep sites. The lack of varnish on the actively growing structures, their weak internal cementation and the lack of sediment drape on the surface deposits all attest to the geologically rapid rate of growth of surface barite deposits. The observation of surface barite deposits that are draped over outcrops of truncated strata devoid of sediment cover (**Figure 5G**) provides further evidence for the geologically fast growth rate of authigenic barite on the seafloor.

Barite Inventory and Barium Sources

Deposits described here are the largest actively forming cold-seep barite deposits documented to date (**Figure 1D**). The mass of barite accumulated on the elongated ridge ($\sim 400 \text{ m} \times 1,000 \text{ m}$) in the SW corner of the mapped area (lower left quadrant **Figure 1D**) amounts to 6.6 million tons of barite, based on 50% coverage of the surface of the ridge by the 11 m tall barite blocks. This is a conservative estimate because the ridge continues to the west farther than the AUV survey reach (**Figure 1B**). The 6.6 million tons of barite found on the $<0.5 \text{ km}^2$ ridge area are comparable to the 5 million tons of barite found in chimneys in the Sea of Okhotsk over a 22 km^2 area (Aloisi et al., 2004). The amount of barite in the whole AUV mapped area is even larger because the calculated inventory of 6.6 million tons of barite does not include all other barite mounds present within the survey (**Figures 1D, 3**).

While the association of the barite mounds and truncated strata is clear, observations in other faults offshore California marking the Pacific Plate-North America Plate boundary, show that faults are often multi-stranded and encompass hundreds of meters wide zones (Johnson and Beeson, 2019). The emergence of barite mounds atop of the ridge could result from the ascent of Ba-rich fluids along a zone of fractures extending the width of the ridge ($\sim 500 \text{ m}$), but too deep to be imaged in the AUV data. Such fluids could be captured by permeable bedding planes. Thus, the association of the mounds and the outcropping bedding planes does not by itself preclude that barium-rich fluids are part of large circulation cells and ultimately migrated from long distance sources along the main fault zone.

A budget calculation is useful to assess whether leaching of San Clemente Basin sediments by fluid circulation is capable of providing sufficient barium to account for the 6.6 million tons of barite found along the ridge. Torres et al., 2002, on the basis of barite $^{87}\text{Sr}/^{86}\text{Sr}$ ratios and the low concentrations of chalcophile elements, suggested that all Ba found in San Clement Fault barite deposits was sourced from the sediment column. The geochemical profile of barite samples measured here is not significantly different from the geochemical composition

of the samples measured by Torres et al. (2002). Thus, in this conservative calculation it is assumed that all Ba in the surface deposits was derived from the sediment column, which dates from the Late Miocene to the present (Teng and Gorsline, 1989), and has a thickness of 400 to 500 m, based on seismic reflection profiles nearby (Normark and Piper, 1972). The sediments that accumulated in the Late Miocene in the California Borderland comprise voluminous diatomaceous sequences (Teng and Gorsline, 1989). Such high-productivity sediments are rich in Ba (Paytan and Griffith, 2007). For example, in the productive Eastern Equatorial Pacific the Ba concentrations in core top sediment are commonly up to 1.5% and sometimes reach 3% (Lyle and Lyle, 2006). Deposition in the California borderland after the Miocene was dominated by clastic inputs (Teng and Gorsline, 1989) with likely lesser Ba content. The thickness of the Late Miocene sequence in the San Clemente Basin is not well known. For simplicity, if it is assumed that the sediment accumulation rate has been constant, Late Miocene (11 to 5 Ma) and younger sediments have 1.5 and 0.2% Ba content, respectively, sediment density is $2,300 \text{ kg/m}^3$, and the area of the sediment pile that is being leached is as large as the surface expression of the surface deposits ($400 \times 1,000 \text{ m}$), then the amount of Ba potentially available under the elongated ridge is ~ 6 million tons of barite, which is equivalent to the amount of barite already accumulated as surface deposits in the mapped area (6.6 million tons). While the deeper pathway of Ba-rich fluids before they reach the seafloor is not known, the current rates of barite growth can be sustained if fluid circulation cells extend wider than the surface expression of the Ba deposits along the fault. This larger inventory of Ba could easily account for the amount of Ba found on the ridge and elsewhere.

CONCLUSION

The world's largest known actively forming cold-seep barite deposit was revealed in a detailed AUV mapping survey along a segment of the San Clemente Fault, where numerous steep sided mounds stand up to 11 m above the surrounding seafloor. These mounds are barite-cemented consolidations of meter-scale rough-textured clumps, which themselves are the remainders of fast accumulating upward branching structures formed by barite aggradation. Despite the large size of the barite blocks and their clustering along a prominent ridge, detection of this morphology at this water depth (962 to 1,300 m) requires a resolution higher than that offered by surface-ship multibeam technology (25 m grid resolution at this depth). Thus, based on the discoveries described here utilizing a high-resolution mapping approach, a plausible hypothesis is that massive barite deposits of the same scale are common along this fault and other faults in the California Borderland where solutions might circulate through organic- and barium-rich sediments. Identification of truncated strata due to fault motion is a useful criterion for the selection of targets where these deposits may occur at other locations offshore Southern California.

DATA AVAILABILITY

The small subunit ribosomal RNA amplicon sequence dataset reported in this study have been deposited in the NCBI Sequence Read Archive (Project No. PRJNA552110).

AUTHOR CONTRIBUTIONS

RG participated in the ROV cruise, did the sample processing and data analyses, and wrote the manuscript. CP conceived and led the project as chief scientist, including the AUV mission planning, ROV cruises participation, data analyses, and manuscript editing. DC led the AUV component including interfacing multibeam and CHIRP instrumentation with the AUV and multibeam and CHIRP data processing. CMP and SJ did 16S DNA analyses and interpretation. EL participated in the ROV cruise, did the AUV data processing and figure drafting and editing. KA participated in the ROV cruise and

did the AUV data processing. All authors commented and edited the manuscript.

ACKNOWLEDGMENTS

The Lucille and David Packard Foundation is acknowledged for their continuous and generous support. Juan Carlos Herguera García at the CICESE (Centro de Investigación Científica y de Educación Superior de Ensenada, México) assisted in securing permission to operate in Mexican waters.

SUPPLEMENTARY MATERIAL

The Supplementary Material for this article can be found online at: <https://www.frontiersin.org/articles/10.3389/fmars.2019.00460/full#supplementary-material>

REFERENCES

- Aloisi, G., Wallmann, K., Bollwerk, S. M., Derkachev, A., Bohrmann, G., and Suess, E. (2004). The effect of dissolved barium on biogeochemical processes at cold seeps. *Geochimica et Cosmochimica Acta* 68, 1735–1748. doi: 10.1016/j.gca.2003.10.010
- Aquilina, L., Dia, A. N., Boulègue, J., Bourgois, J., and Fouillac, A. M. (1997). Massive barite deposits in the convergent margin off peru: implications for fluid circulation within subduction zones. *Geochimica et Cosmochimica Acta* 61, 1233–1245. doi: 10.1016/S0016-7037(96)00402-4
- Bergquist, D. C., Williams, F. M., and Fisher, C. R. (2000). Longevity record for deep-sea invertebrate. *Nature* 403, 499–500. doi: 10.1038/35000647
- Canet, C., Anadón, P., Alfonso, P., Prol-Ledesma, R. M., Villanueva-Estrada, R. E., and García-Vallès, M. (2013). Gas-seep related carbonate and barite authigenic mineralization in the northern Gulf of California. *Mar. Pet. Geol.* 43, 147–165. doi: 10.1016/j.marpetgeo.2013.02.011
- Caporaso, J. G., Kuczynski, J., Stombaugh, J., Bittinger, K., Bushman, F. D., Costello, E. K., et al. (2010). QIIME allows analysis of high-throughput community sequencing data. *Nat. Methods* 7, 335–336. doi: 10.1038/nmeth.1303
- Caporaso, J. G., Lauber, C. L., Walters, W. A., Berg-Lyons, D., Lozupone, C. A., Turnbaugh, P. J., et al. (2011). Global patterns of 16S rRNA diversity at a depth of millions of sequences per sample. *Proc. Natl. Acad. Sci. U.S.A.* 108(Suppl. 1), 4516–4522. doi: 10.1073/pnas.1000080107
- Caress, D. W., Thomas, H., Kirkwood, W. J., McEwen, R., Henthorn, R., Clague, D. A., et al. (2008). “High-Resolution multibeam, sidescan, and subbottom surveys using the MBARI AUV D. Allan B,” in *Marine Habitat Mapping Technology for Alaska*, eds J. R. Reynolds and H. G. Greene (Fairbanks, AK: University of Alaska Fairbanks).
- Carvajal, C., Paull, C. K., Caress, D. W., Fildani, A., Lundsten, E., Anderson, K., et al. (2017). Unraveling the channel-lobe transition zone with high-resolution AUV bathymetry: navy fan, offshore baja california, mexico. *J. Sediment. Res.* 87, 1049–1059. doi: 10.2110/jsr.2017.58
- Clark, S. H. B., Poole, F. G., and Wang, Z. (2004). Comparison of some sediment-hosted, stratiform barite deposits in China, the United States, and India. *Ore Geol. Rev.* 24, 85–101. doi: 10.1016/j.oregeorev.2003.08.009
- Dhillon, A., Teske, A., Dillon, J., Stahl, D. A., and Sogin, M. L. (2003). Molecular characterization of sulfate-reducing bacteria in the guaymas basin. *Appl. Environ. Microbiol.* 69, 2765–2772. doi: 10.1128/AEM.69.5.2765-2772.2003
- Fang, J. K. H., Rooks, C. A., Krogness, C. M., Kutti, T., Hoffmann, F., and Bannister, R. J. (2018). Impact of particulate sediment, bentonite and barite (oil-drilling waste) on net fluxes of oxygen and nitrogen in arctic-boreal sponges. *Environ. Poll.* 238, 948–958. doi: 10.1016/j.envpol.2017.11.092
- Feng, D., and Roberts, H. H. (2011). Geochemical characteristics of the barite deposits at cold seeps from the northern Gulf of Mexico continental slope. *Earth Planet. Sci. Lett.* 309, 89–99. doi: 10.1016/j.epsl.2011.06.017
- Greiner, J., Bollwerk, S. M., Derkachev, A., Bohrmann, G., and Suess, E. (2002). Massive barite deposits and carbonate mineralization in the Derugin Basin, Sea of Okhotsk: precipitation processes at cold seep sites. *Earth Planet. Sci. Lett.* 203, 165–180. doi: 10.1016/S0012-821X(02)00830-0
- Hein, J. R., Zierenberg, R. A., Maynard, J. B., and Hannington, M. D. (2007). Barite-forming environments along a rifted continental margin, Southern California Borderland. *Deep Sea Res. II: Top. Stud. Oceanogr.* 54, 1327–1349. doi: 10.1016/j.dsr2.2007.04.011
- Holmden, C., Creaser, R. A., and Muehlenbachs, K. (1997). Paleosalinities in ancient brackish water systems determined by 87Sr/86Sr ratios in carbonate fossils: a case study from the Western Canada sedimentary basin. *Geochimica et Cosmochimica Acta* 61, 2105–2118. doi: 10.1016/S0016-7037(97)00073-2
- Johnson, S. B., Krylova, E. M., Audzijonyte, A., Sahling, H., and Vrijenhoek, R. C. (2017). Phylogeny and origins of chemosynthetic vesicomyid clams. *Systemat. Biodivers.* 15, 346–360. doi: 10.1080/14772000.2016.1252438
- Johnson, S. Y., and Beeson, J. W. (2019). Shallow structure and geomorphology along the offshore northern san andreas fault, tomales point to fort ross, californiashallow structure and geomorphology along the offshore northern san andreas fault. *Bull. Seismol. Soc. Am.* 109, 833–854. doi: 10.1785/0120180158
- Koski, R. A., and Hein, J. R. (2004). *Stratiform Barite Deposits in the Roberts Mountains Allochthon, Nevada: A Review Of Potential Analogs in Modern Sea-Floor Environments*. Nevada, NV: US Geological Survey.
- Langseth, M. E., Mottl, M. A., Hobart, M. A., and Fisher, A. (1988). The distribution of gethermal and geochemical gradients near site 501/504: implications for hydrothermal circulation in the oceanic crust. *Proc. Ocean Drill. Prog.* 111, 23–32. doi: 10.2973/odp.proc.ir.111.1988
- Lonsdale, P. (1979). A deep-sea hydrothermal site on a strike-slip fault. *Nature* 281, 531–534. doi: 10.1038/281531a0
- Lyle, A. O., and Lyle, M. L. (2006). Organic carbon and barium in eocene sediments: possible controls on nutrient recycling in the eocene equatorial pacific ocean. *Proc. Ocean Drill. Prog. Sci. Res.* 199, 1–33. doi: 10.2973/odp.proc.sr.199.2006
- Naehr, T. H., Stakes, D. S., and Moore, W. S. (2000). Mass wasting, ephemeral fluid flow, and barite deposition on the California continental margin. *Geology* 28, 315–318. doi: 10.1130/0091-7613(2000)028<0315:mweffa>2.3.co;2
- Normark, W. R., and Piper, D. J. W. (1972). Sediments and growth pattern of navy deep-sea fan, san clemente basin, california borderland. *J. Geol.* 80, 198–223. doi: 10.1086/627725
- Parada, A. E., Needham, D. M., and Fuhrman, J. A. (2016). Every base matters: assessing small subunit rRNA primers for marine microbiomes with mock

- communities, time series and global field samples. *Environ. Microbiol.* 18, 1403–1414. doi: 10.1111/1462-2920.13023
- Paull, C. K., Chanton, J. P., Neumann, A. C., Coston, J. A., Martens, C. S., and Showers, W. (1992). Indicators of methane-derived carbonates and chemosynthetic organic carbon deposits: examples from the florida escarpment. *PALAIOS* 7, 361–375. doi: 10.2307/3514822
- Paytan, A., and Griffith, E. M. (2007). Marine barite: recorder of variations in ocean export productivity. *Deep Sea Res. II: Top. Stud. Oceanogr.* 54, 687–705. doi: 10.1016/j.dsr2.2007.01.007
- Revelle, R., and Emery, K. O. (1951). Barite concretions from the seafloor. *GSA Bull.* 62, 707–724.
- Salman-Carvalho, V., Fadeev, E., Joye, S. B., and Teske, A. (2016). How clonal is clonal? genome plasticity across multicellular segments of a “*Candidatus Marithrix* sp.” filament from sulfidic, briny seafloor sediments in the Gulf of Mexico. *Front. Microbiol.* 7. doi: 10.3389/fmicb.2016.01173
- Schauer, R., Røy, H., Augustin, N., Gennerich, H.-H., Peters, M., Wenzhoefer, F., et al. (2011). Bacterial sulfur cycling shapes microbial communities in surface sediments of an ultramafic hydrothermal vent field. *Environ. Microbiol.* 13, 2633–2648. doi: 10.1111/j.1462-2920.2011.02530.x
- Snyder, G. T., Dickens, G. R., and Castellini, D. G. (2007). Labile barite contents and dissolved barium concentrations on Blake ridge: new perspectives on barium cycling above gas hydrate systems. *J. Geochem. Explor.* 95, 48–65. doi: 10.1016/j.gexplo.2007.06.001
- Suess, E., Bohrmann, G., Huene, R., von Linke, P., Wallmann, K., Lammers, S., et al. (1998). Fluid venting in the eastern Aleutian subduction zone. *J. Geophys. Res: Solid Earth* 103, 2597–2614. doi: 10.1029/97JB02131
- Teng, L. S., and Gorsline, D. S. (1989). Late Cenozoic sedimentation in California continental borderland basins as revealed by seismic facies analysis. *GSA Bull.* 101, 27–41. doi: 10.1130/0016-7606(1989)101<0027:lcsicc>2.3.co;2
- Thompson, L. R., Sanders, J. G., McDonald, D., Amir, A., Ladau, J., Locey, K. J., et al. (2017). A communal catalogue reveals Earth's multiscale microbial diversity. *Nature* 551, 457–463. doi: 10.1038/nature24621
- Torres, M. E., Bohrmann, G., Dubé, T. E., and Poole, F. G. (2003). Formation of modern and Paleozoic stratiform barite at cold methane seeps on continental margins. *Geology* 31, 897–900. doi: 10.1130/G19652.1
- Torres, M. E., Bohrmann, G., and Suess, E. (1996a). Authigenic barites and fluxes of barium associated with fluid seeps in the Peru subduction zone. *Earth Planet. Sci. Lett.* 144, 469–481. doi: 10.1016/S0012-821X(96)00163-X
- Torres, M. E., Brumsack, H. J., Bohrmann, G., and Emeis, K. C. (1996b). Barite fronts in continental margin sediments: a new look at barium remobilization in the zone of sulfate reduction and formation of heavy barites in diagenetic fronts. *Chem. Geol.* 127, 125–139. doi: 10.1016/0009-2541(95)00090-9
- Torres, M. E., McManus, J., and Goldfinger, C. (2000). *Mapping, Geochemical Sampling and Submersible Observations of Recent Activity on the San Clemente Fault Zone* (No. 180 00-4). Corvallis, OR: College of Oceanic & Atmospheric Sciences.
- Torres, M. E., McManus, J., and Huh, C.-A. (2002). Fluid seepage along the San Clemente fault scarp: basin-wide impact on barium cycling. *Earth Planet. Sci. Lett.* 203, 181–194. doi: 10.1016/S0012-821X(02)00800-2

Conflict of Interest Statement: The authors declare that the research was conducted in the absence of any commercial or financial relationships that could be construed as a potential conflict of interest.

Copyright © 2019 Gwiazda, Paull, Caress, Preston, Johnson, Lundsten and Anderson. This is an open-access article distributed under the terms of the Creative Commons Attribution License (CC BY). The use, distribution or reproduction in other forums is permitted, provided the original author(s) and the copyright owner(s) are credited and that the original publication in this journal is cited, in accordance with accepted academic practice. No use, distribution or reproduction is permitted which does not comply with these terms.